Application of Functionally Graded Materials for Severe Plastic Deformation and Smart Materials
—Experimental Study and Finite Element Analysis—

巨大ひずみ加工およびスマートマテリアルへの傾斜機能材料技術の応用
—有限要素法解析および実験的検証—

Thesis submitted to
Graduate School of Engineering,
Nagoya Institute of Technology.
Doctor degree of engineering.

by
Saifulnizan Jamian

Supervisors
Prof. Yoshimi Watanabe
Assoc. Prof. Hisashi Sato

Department of Engineering Physics, Electronics and Mechanics

2012

Abstract

Functionally graded materials (FGMs) refer to the composite materials where the compositions or the microstructures are locally varied so that a certain variation of the local material properties is achieved. Determination of compositional gradient and the process of making an FGM are dependent on its intended use. In this study, new possible applications of FGM and its production process were investigated. Three possible application of FGM were proposed.

First, the novel technique in producing ultra fine grain of difficult-to-work materials by equal-channel angular pressing (ECAP) process at ambient temperature was developed by using FGM. For this study, Ti as the difficult-to-work material was tightly encapsulated in a hollow host material made of Al-based FGM matrix. The Al-based FGM as a host material assists the deformation of Ti. The ECAP process was simulated by the finite element method (FEM) to determine the appropriate compositional gradient of Al-based FGM and the position to embed Ti wire. FEM was conducted with Ti embedded into a different host material type as well as different die channel geometry. The strain distribution of the specimen after a single ECAP pass was analyzed. From the obtained results, it is found that the strain distribution in Ti is strongly influenced by the host material and the shape of the die channel. An experimental work was carried out to confirm the ability of the proposed technique in producing ultra fine grain of Ti. The host material was prepared by embedding Al-Al_3Ti alloy into Al. Three types of the Al-Al_3Ti alloys with different Al_3Ti volume fractions were used to prepare the host materials. ECAP for specimens was carried out for up to eight passes by route A. The microstructure and hardness of ECAPed specimens were investigated. The changes in microstructure and the increase in the hardness value of Ti with increased number of ECAP passes are evidences showing that Ti is successfully deformed by this technique.

Second, new types of FGM crash boxes with stepwise strength gradient in longitudinal directions were proposed. The property of the proposed FGM crash boxes were analyzed using FEM. Crash behavior of the crash box under axial quasi-static and dynamic impact loads were studied. The obtained load-displacement curves and the crash failure patterns then were evaluated to assess the effect of the stepwise strength gradient of the crash-box.

Moreover, four different shapes of cross-sectional i.e. square, circle, pentagon and hexagon were considered. The results show that the FGM crash box is superior to than the homogeneous crash box in overall crashworthiness. Although there were no trigger mechanism introduced, the FGM crash boxes experience the progressive crushing initiated at the impact side.

Third, the FGMs were applied in pipe and pressure vessel field. A solution procedure for finite element thermo-visco-plasticity and creep analysis in an FGM thick-walled pressure vessel subjected to thermal and internal pressure was presented. The thick-walled pressure vessel was replaced by a system of discrete rectangular cross-section ring elements interconnected along circumferential nodal circles. The property of FGM was assumed to be continuous function of volume fraction of material composition. The thermo-visco-plasticity and creep behavior of the structures were obtained by the use of an incremental approach. The obtained results show that the material composition significantly affects the stress as a function of time at the inside and outside surface of thick-walled pressure vessel. The use of FGM can adjust the stress distribution in the structure.

Moreover, one of the FGM fabrication method, centrifugal casting, was investigated. Two types of centrifugal casting method namely, centrifugal solid-particle method (CSPM) and centrifugal mixed-powder method (CMPM), were used to fabricate Al/SiC FGM. Formations of graded distribution of SiC particles within molten Al by CSPM and CMPM under huge centrifugal force were examined and simulated. The movement of SiC particles in viscous liquid under centrifugal force was explained theoretically based on Stoke's law. The effect of composition gradient of particles on viscosity was taken into account. Also, the effect of temperature distribution on viscosity and density were considered. A computer code to simulate the formation of compositional gradient in an Al/SiC FGM manufactured by CSPM and CMPM was developed. From the obtained results, it was found that the SiC particles can be graded from inner to outer surface of Al/SiC FGM by CSPM. Meanwhile by CMPM, the SiC particles can be dispersed on the surface of Al/SiC FGM. The graded distribution in Al/SiC FGM under huge centrifugal force was significantly affected by the mold temperature but less affected by the initial temperature of molten Al and casting atmosphere.

Table of Contents

Chapter 1

Introduction and Literature Survey

1.1 Functionally Graded Materials

Functionally graded materials (FGMs) refer to the composite materials where the composition or the microstructure is locally varied so that a certain variation of the local material properties is achieved. The materials can be designed for specific function and applications. Various approaches based on the bulk (particulate processing), preform processing, layer processing and melt processing are used to fabricate the FGMs [1]. The concept of FGM was fist considered in Japan in 1984 during a space plane project. That time the aim is to fabricate a space plane body's material with improved thermal resistance and mechanical properties by gradually changing (grading) compositions. Therefore, the space plane body is resistant to severe condition from temperature gap (about 1000 deg. C gap) in between the inside and the outside.

The structural unit of an FGM is referred to as an element or a material ingredient [1]. It is a conceptual unit for constructing an FGM that includes various aspects of its chemical composition, physical state and geometrical configuration. According to Miyamoto et al. [1] the term material ingredient, probably expresses the overall concept best. Generally, there are two main types of FGMs i.e. continuous graded materials and discontinuous graded materials. In the simplest FGMs, two different material ingredients change gradually from one to the other as illustrated in Fig. 1.1(a). In the second type, the material ingredients change in a discontinuous way such as the stepwise gradation illustrated in Fig. 1.1(b).

A material can be considered to be an FGM even if the gradation of the material ingredients is limited to a specific location in the material such as the interface, a joint, or a surface. As long as the material incorporates the FGM concept it can be categorized as an FGM. Therefore, an FGM can be produced from a homogeneous material and then processed with different condition such as heat treatment and deformation.

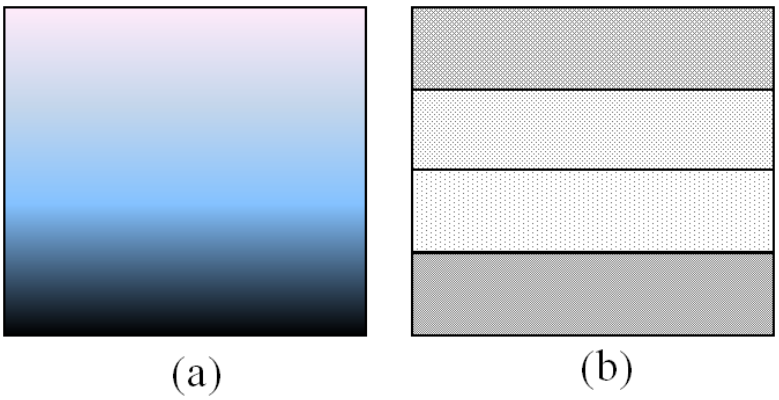

Fig. 1.1 Type of FGM structure: (a) continuous and (b) discontinuous.

1.2 Manufacturing Process of FGMs

There is wide variety of processing methods to fabricate FGMs available today [1–4]. The processing methods can be classified into those based on constructive processing and those based on mass transport [2]. In the first class, the FGM is constructed layer-by-layer starting with an appropriate distribution of the FGM's constituents. These techniques are called constructive processes because gradients are literally constructed in space. Meanwhile in the second class of FGM process, the gradients within a components are depend on natural transport phenomena such as the flow of fluid, the diffusion of atomic species, or the conduction of heat. FGMs can be manufactured by centrifugal casting [3], sequential slip casting [5], thermal spraying [6], physical vapour deposition (PVD) [7], chemical vapour deposition (CVD) [7] and laser cladding [8].

Powder metallurgy, a constructive processing method, is a one of the most important methods of producing FGMs. Generally, this method consists of three main steps. At first, materials desired in powder form are weighed and mixed. Next step is stepwise staking of premixed powder according to a predesigned spatial distribution of the composition. Last step is a sintering. By this method, the FGM fabricated usually have the stepwise structure, and it is difficult to produce the FGM with continuous gradient.

An example of natural transport phenomena method is centrifugal method. FGMs are fabricated under a centrifugal force, by which it is possible to produce the FGMs

with continuous gradients. Fabrication methods of FGMs under the centrifugal force are classified into three categories, namely centrifugal method (application of centrifugal casting), centrifugal slurry method (centrifugal sedimentation) and centrifugal pressurization method (simple pressurization by the centrifugal force). In case of centrifugal method, a centrifugal force applied to a homogeneous molten metal, dispersed with ceramics particles or intermetallic compound particles, drives the formation of the desired gradation. The composition gradient is then achieved primarily by the difference in the centrifugal force produced by the difference in density between the molten metal and solid particles [9, 10]. It is known that the motion of particles in a viscous liquid under a centrifugal force obeys the Stokes' law [10–12].

In contrast, slurry with two types of solid particles, high-velocity particle and low-velocity particle, is subjected to the centrifugal force during the fabrication of FGMs by the centrifugal slurry method [13]. After complete sedimentation occurs, liquid part of the slurry will be removed, and therefore, it does not become a part of FGM. Third one is the centrifugal pressurization method, by which the centrifugal force is only used for simple pressurization. In this method, compositional gradation should be formed prior the application of centrifugal force [14, 15].

1.3 Application of FGMs

Nowadays the researches on FGMs have been carried out intensively. Since the concept developed in aeronautics field in 1984, FGMs are also a concern in the other fields such as industrial materials, optoelectronics, biomaterials, and energy materials. FGMs offer great promise in applications where the operating conditions are severe. Potential applications include those structural and engineering uses that require combinations of incompatible functions such as refractoriness or hardness with toughness or chemical inertness with toughness. In aerospace and nuclear energy applications, reliability rather than cost is the key issue. On the other hands, in applications such as cutting tools, machine parts and engine components, which require wear, heat, mechanical shock and corrosion resistance, the key issues are the cost/performance ratio and reliability. Examples of available commercial FGM products are high performance cutting tools of

tungsten carbide/cobalt based FGMs and razor blades of an iron aluminide/stainless steel FGM [1].

There are many potentially useful applications of the FGM concept which is not limited to the fields discussed in this report as well as the manufacturing processes of FGMs. In this study, three possible applications of FGMs were discussed. For the two first proposed applications, the stepwise gradations FGMs were used. Meanwhile for the third proposed application, the continuous graded materials were chosen to be applied in tube and pressure vessel field.

1.4 Experimental and Numerical Approach

In analyzing the possible applications of FGMs proposed in this study both experimental and numerical works were carried out. In engineering applications, there are many types of numerical method that usually used such as finite difference method (FDM), finite volume method (FVM), finite element method (FEM), boundary element method (BEM) and mesh-free method. However in this study, for the numerical analysis only FEM was considered. FEM are widely used in diverse fields to solve static and dynamic problems. The advantages and disadvantages of FEM are listed in Table 1.1

In FEM the solution procedure is very typical. The main steps in implementation of FEM are summarized as follow:

a) Discretization of the domain into a set of finite elements.
b) Defining an approximate solution over the element.
c) Weighted integral formulation of the differential equation.
d) Substitute the approximate solution and get the algebraic equation

Table 1.1 Advantages and disadvantages of FEM

Advantages	Disadvantages
Able to handle very complex geometry	A general closed-form solution, which would permit one to examine system response to changes in various parameters, is not produced.
Able to solve a wide variety of engineering problems	The results obtains only "approximate" solutions
Able to handle complex restraints	It has "inherent" errors.
Able to handle complex loading	Mistakes by users can be fatal.

The main challenge to implement FEM in analyzing FGMs structures is to describe the material properties of FGMs. To describe the material properties of FGMs by theoretical approach is not easy. The estimation of material properties for phase composites by theoretical approaches are split into microscopic and overall studies. The prediction methods of overall material properties are generally classified into three group i.e direct, variational and approximation approaches. The direct method seeks closed-form analytic solution. Therefore a precise mathematical treatment becomes troublesome. On the other hand, the variational method such as Hashin Shtrikman's bounds does not specify the details in the phase geometry but rather provide the upper and lower bounds for the overall properties. In the approximation approach, the self-consistent model by Hill and the others, the mean field micro-mechanics models by Mori and Tanaka and Wakashima and Tsukamoto, the linear and modified rules of mixtures by Tamura and the unit cell model by Ravichandran are widely employed overall estimation [1–3]. The overall models are simple and convenient to predict the overall thermo-mechanical response and material properties. However, in this study, the conventional modeling of FGMs, the rule of mixture is considered. Although, the macroscopic properties of FGMs cannot be accurately described by the rule of mixture,

but by dividing the FGMs structure into significantly small size of mesh and the material properties considered at every integration points is gives reasonable results when analyzing the FGMs structure by FEM.

In this study, FEM is used to determine the appropriate FGMs structure for the proposed application to reduce number of experimental works carried out. Experimental work still required to be performed in order to prove the workability of the proposed FGMs applications.

1.5 Thesis outline

In Chapter 2, the novel technique in producing ultra fine grain of difficult-to-work materials by ECAP process at ambient temperature was developed by using FGM. The ECAP process was simulated by the FEM to determine the appropriate compositional gradient of Al-based FGM and the position to embed Ti wire.

In Chapter 3, an experimental work was carried out to confirm the ability of the proposed technique in producing ultra fine grain of Ti. The microstructure and hardness of ECAPed specimens were investigated.

In Chapter 4, new types of FGM crash boxes with stepwise strength gradient in longitudinal directions were proposed. Finite element analysis was performed in order to determine the crash behavior of the crash boxes. The crashworthiness characteristics of FGM crash boxes were discussed.

Chapter 5 discussed the possible application of FGM in pipe and pressure vessels field. The analysis of thermo-visco-plasticity and creep characteristics of the FGM thick-walled pressure vessels were carried out using FEM. The obtained results show that the use of FGMs can adjust the stress distribution in the structure.

Finally Chapter 6 describes the promising mass manufacturing of FGMs, centrifugal casting. The fabrications of Al/SiC FGM using two types of centrifugal casting method namely, solid-particle method and mixed-powder method, were carried out. The formation of graded distribution of SiC particles within molten Al by centrifugal solid-particle method and centrifugal mixed-powder method were examined and simulated.

Chapter 7 present the overall conclusion and recommendation for future work in this research area.

References

1) Y. Miyamoto, W.A. Kaysser, B.H. Rabin, A. Kawasaki, and R.G. Ford: Functionally Graded Materials: Design, Processing and Applications, Kluwer Academic, Boston (1999).
2) S. Suresh and A. Mortensen: Fundamental of Functionally Graded Materials, The University Press, Cambridge (1998).
3) A. Neubrand and J. Rödel. Gradient Materials: An overview of a novel concept. Z. fur Metallkunde. **5(88)** (1997) 358.
4) Y. Watanabe and H. Sato: Review Fabrication of Functionally Graded Materials under a Centrifugal Force, Nanocomposites with Unique Properties and Applications in Medicine and Industry (2011) 133.
5) J.S. Moya, J.A. Sánchez-Herencia, J. Requena, and R. Moreno: Mat. Let. **14**(1992) 333.
6) J. Musil and J. Fiala: Surface and Coating Technology **52** (1992) 211.
7) D.C. Sun, E.Y. Yiang, S. Liu Ming, and C. Lin: J.Phys. D: Applied Physics **28** (1995) 4.
8) K.M. Jasim, R.D. Rawlings, and R.F. West: J. Mater. Sci. 43(1-4) (1993) 2820.
9) Y. Fukui: JSME Int. J. Series III, **34 (1)** (1991) 144.
10) Y. Watanabe, N. Yamanaka, and Y. Fukui: Comp. A **29A** (1998) 595.
11) C.G. Kang and P.K. Rohatgi: Metall Mater Trans B **27B** (1996) 277.
12) T. Ogawa, Y. Watanabe, H. Sato, I.S. Kim, and Y. Fukui: Comp. A **37** (2006) 2194.
13) Watanabe, E. Miura-Fujiwara, and H. Sato: J. Jpn. Soc. Powder Powder Metall. **57** (2010) 321.
14) Y. Watanabe, S. Watanabe, and K. Matsuura: Metall. Mater. Trans. A **35A** (2004) 1517.
15) Y. Watanabe, Y. Inaguma, H. Sato, and E. Miura-Fujiwara: Mater. **2** (2009) 2510.

Chapter 2

Finite Element Analysis of Severe Plastic Deformation of Difficult-to-Work Material by Equal-Channel Angular Pressing at Ambient Temperature

2.1 Introduction

Equal-channel angular pressing (ECAP) invented by Segal et al.[1] in 1977 is one of the severe plastic deformation (SPD) techniques, which has great potential for producing ultrafine grain materials in bulk. Figure 2.1 shows a schematic illustration of ECAP process. As shown in Fig. 2.1, the ECAP process is performed by pressing a specimen through a die consisting of two intersecting channels meeting at an angle ϕ and outer corner meeting at an angle φ. This process has the advantage that a large plastic strain can be induced without changing the cross section of the specimen. Because of it, a larger plastic strain is imposed by repeating several passes. In addition, the ECAP process has four standard routes: route A (no rotation), route B_A (90° back and forth rotation between passes), route B_C (90° in the same direction between passes), and route C (180° in the same direction between passes). Therefore, the property of the induced strain can be controlled by the processing route.

In the case of the deformation of a high-strength material using ECAP, an elevated temperature is often required [2, 3]. In particular, Ti alloys are difficult to deform, and a higher pressing-temperature is required to increase their ductility during the deformation. This is because Ti and Ti alloys have limited numbers of slip systems owing to the crystal having a hexagonal close packed (hcp) structure [4, 5]. In previous studies, the ECAP process for Ti has been performed under elevated temperatures [3–8]. In previous studies, this ECAP process for Ti was carried out at elevated temperatures up to 450 °C, and they suggested that the lowest temperature for deforming Ti successfully was 200 °C [8]. Therefore, it is very difficult to deform Ti by ECAP at room temperature.

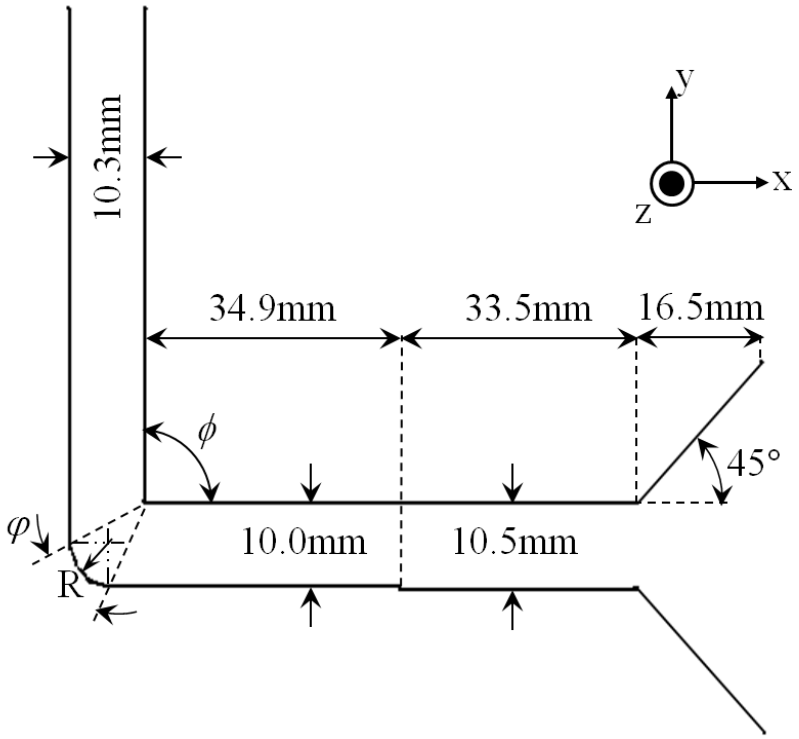

Fig. 2.1 ECAP die geometry featuring the die angle ϕ, outer corner angle φ, and outer fillet radius R.

Recently, the present authors have proposed a new technique of ECAP at ambient temperature [9]. The proposed ECAP process is carried out by embedding a difficult-to-work material into an easy-to-work material. According to our previous study, Ti (difficult-to-work material) has been successfully deformed by embedding it into pure Al (easy-to-work material) at room temperature. However, the proposed method has the problem that a crack is generated at the interface between Ti and pure Al during ECAP. In order to solve this problem, it is considered that the easy-to-work material should be an Al-based alloy or an Al-based functionally graded material (FGM). This is because it is better to decrease the difference in mechanical property between the difficult-to-work material and the easy-to-work material. Moreover, the amount of strain induced in Ti by the proposed ECAP is still unclear.

In this study, a comprehensive examination of the deformation of a difficult-to-work material using ECAP at room temperature is carried out by the finite element method (FEM). For this study, Ti as the difficult-to-work material is embedded into an Al-based alloy and an Al-based FGM matrix. The strain distribution in a specimen induced with single-pass ECAP depending on the position of Ti, the material for the matrix, and the geometry of die channels are discussed. From the obtained results, the capability of the proposed ECAP process to deform difficult-to-work materials is also discussed.

2. 2 FEM Analysis for the Strain Distribution in Specimen Induced by ECAP

FEM simulation was performed using the implicit finite element code Marc. The solution procedure is based on the full Newton-Raphson iterative-increment procedure. For the convergence criteria, the relative displacement criterion and relative residual force criterion are used, and convergence is obtained if one converges. Two-dimensional plane strain modeling is applied since material flow in the z-direction is restricted [10] for a single ECAP pass. A plane representing the ECAP specimen was divided into a mesh of 1200 equal four-node quadrilateral elements with 21 nodes in the x-direction and 61 nodes in the y-direction. The frictional coefficient between the die channel inside and the specimen is assumed to be zero because the specimen is lubricated during the experiment of ECAP. The geometry of the die channel is also shown in Fig. 2.1. The die channel and puncher made of die steel (DC53) produced by Daido Steel Co, Ltd. were considered to be rigid. The puncher moved down along the inlet channel at a constant velocity of 4 mm/s. To describe briefly the experiment of ECAP, the dummy specimen is used to push the specimen out of the die channels. After being pressed by the puncher for 50 mm, the specimen is pushed out by the dummy specimen. The schematic process of ECAP is shown in Fig. 2.2.

Figure 2.3 shows two types of specimen used in this simulation. For one specimen shown in Fig. 2.3(a), Ti with a length of 20 mm and a width of 1 mm is embedded at the end of the host material. The other specimen shown in Fig. 2.3(b) has the structure in which Ti is embedded in the middle of the host material. The host material is either an alloy or FGM with gradient strength. The FGM matrix is made by combining two

different Al alloys with the higher-strength alloy on the inner side, as defined in Table 2.1. The dimensions of the host material are 60 mm in length and 10 mm in width, and for the FGM matrix, the second layer is 40 mm in length and 5 mm in width. In the simulation, each material is defined as a different deformable body. For simplicity, the nodes at the interface belong to both materials and the separation of nodes is not considered.

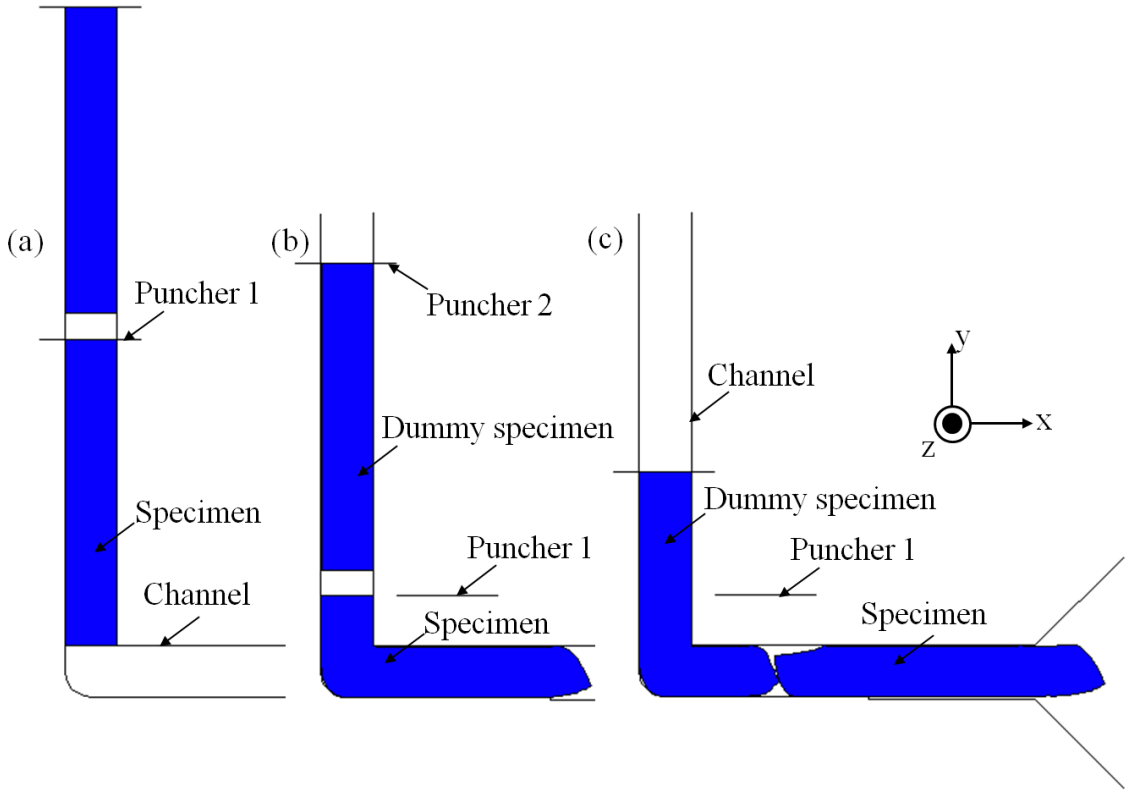

Fig. 2.2 ECAP process: (a) the initial deformation stage, (b) during steady-state of ECAP, and (c) the final stage after ECAP.

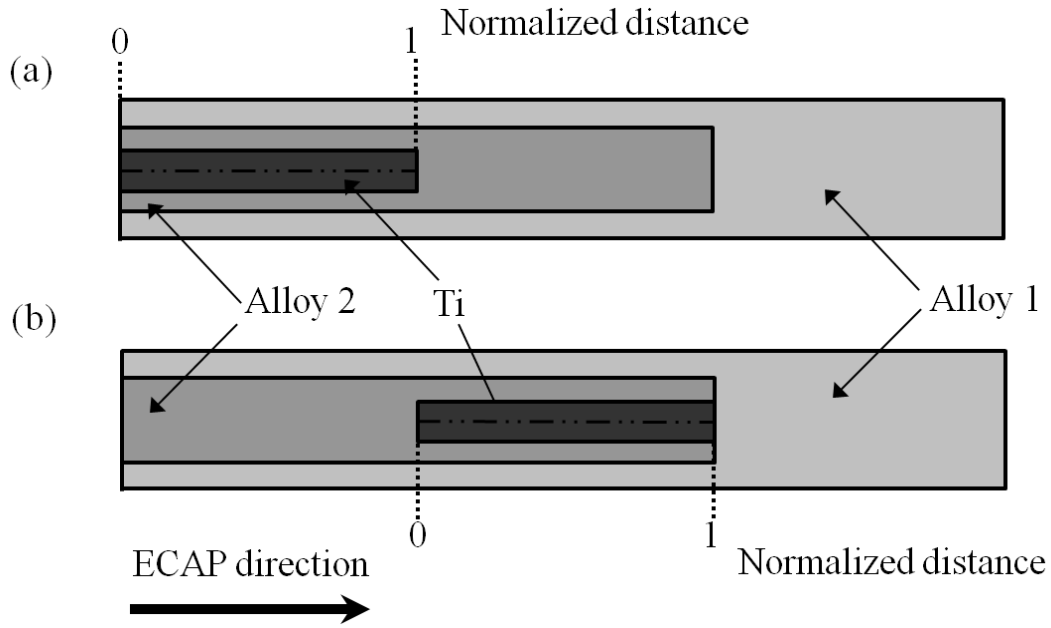

Fig. 2.3 Schematic of ECAP specimens: (a) Ti embedded at the end and (b) Ti embedded in the middle of specimen. The representative line defined along Ti is indicated.

As listed in Table 2.1, pure Al, Al-5%Ti, and Al-10%Ti are used as the host materials. The material properties of Al-5%Ti and Al-10%Ti are determined from the material properties of pure Ti and Al on the basis of the law of mixture. Although these material properties are inaccurately described, it is adequate to show the different strengths of these alloys used in this simulation. Young's modulus, *E*, Poisson's ratio, ν, and yield stress, σ^y, for Al are 71 GPa, 0.33, and 22.5 MPa, respectively. On the other hand, *E*, ν, and σ^y for Ti are 116 GPa, 0.32, and 140 MPa, respectively. The strain hardening for both materials can be presented as follows,

$$\sigma_{Al} = \sigma_{Al}^{y}\left[1+3.5\left(\varepsilon^{P}\right)^{0.7}\right], \tag{2.1}$$

$$\sigma_{Ti} = \sigma_{Ti}^{y}\left[1+\left(\varepsilon^{P}\right)^{0.25}\right], \tag{2.2}$$

where σ is the flow stress and ε^P denotes the equivalent plastic strain.

Table 2.1 List of the specimens defined on the basis of Fig. 2.3.

Sample	Alloy 1	Alloy 2
H1	Al	Al
H2	Al-5 mass%Ti	Al-5 mass%Ti
H3	Al-10 mass%Ti	Al-10 mass%Ti
FGM1	Al	Al-5 mass%Ti
FGM2	Al	Al-10 mass%Ti
FGM3	Al-5 mass%Ti	Al-10 mass%Ti

Firstly, the finite element calculation was validated by comparing with analytical solution. Since the frictional effect is neglected, the obtained results can be compared with equivalent strain presented in following equation [11]

$$\varepsilon = \frac{1}{\sqrt{3}}\left[2\cot\left(\frac{\phi}{2}+\frac{\varphi}{2}\right)+\varphi\,\mathrm{cosec}\left(\frac{\phi}{2}+\frac{\varphi}{2}\right)\right]. \tag{2.3}$$

In this equation, ϕ = 90° and φ = 37.5°, which corresponds to R = 5.15 mm, were considered as the size of the ECAP die. The equivalent strain estimated using Eq. (2.3) is 0.99 while the obtained value calculated by FEM is 1.08. This estimated value is in good agreement with that calculated by FEM. This means that the present FEM analysis is valid as the analysis method for strain distribution in ECAPed specimens.

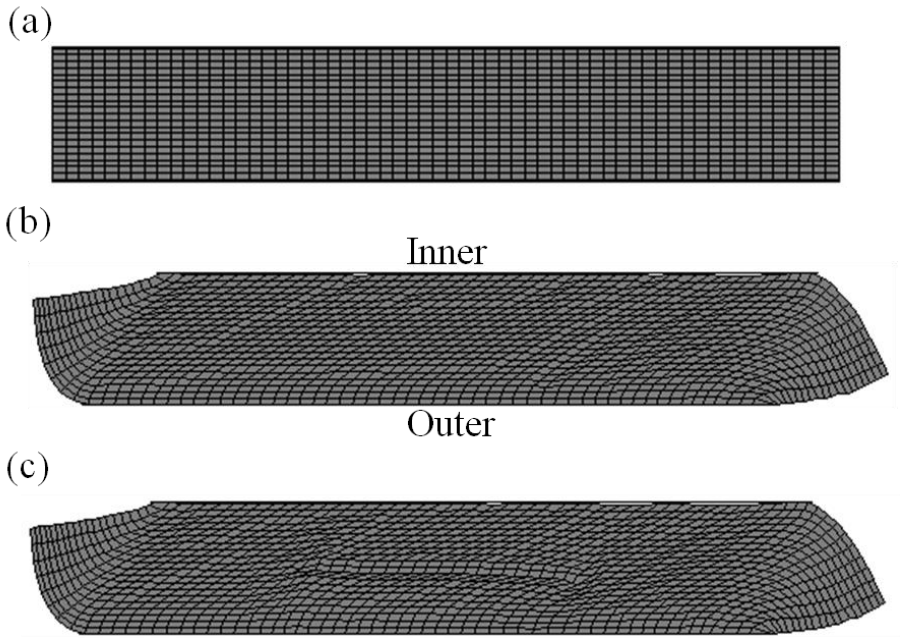

Fig. 2.4 Deformed geometry changes during ECAP: (a) Before ECAP; (b) and (c) after single pass of pure Al without and with Ti embedded, respectively.

Figure 2.4 shows the comparison of deformed geometry after a single ECAP pass. As shown in Fig. 2.4, the equal-quadrilateral-element mesh is distorted by passing through the angular shear zone. Moreover, it is seen from Fig. 2.4(b) that shear deformation in the outer part of the ECAP sample is smaller than in another part. This is in agreement with the results of previous studies [2, 12–15].

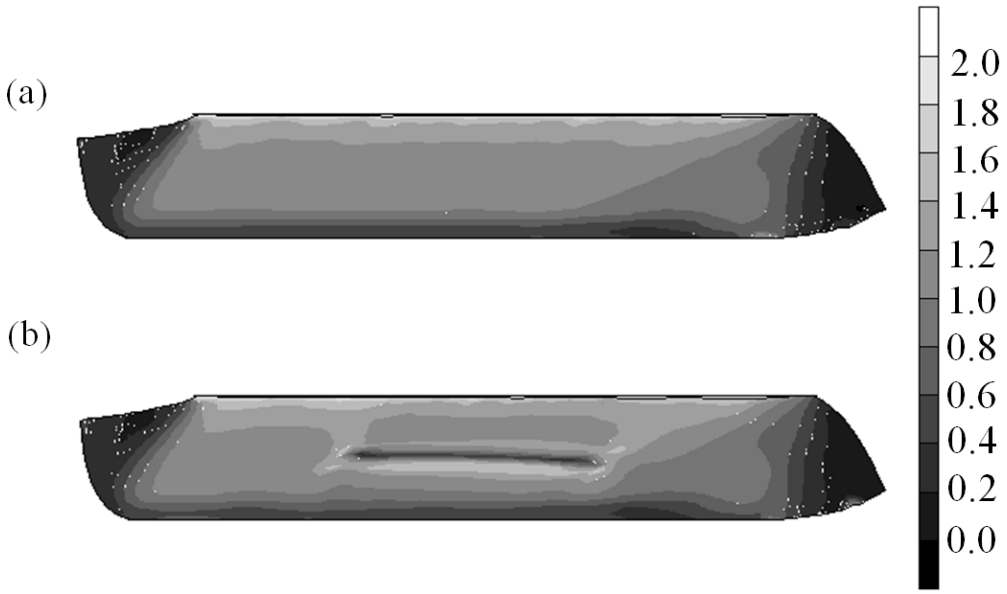

Fig. 2.5 Comparison of distribution of the equivalent strain in the specimen after single ECAP pass: (a) pure Al and (b) Ti embedded in pure Al (H1).

The deformation of a specimen during the ECAP process is inhomogeneous. The calculated strain varies along the specimen axis and the transverse direction from top to bottom. Figure 2.5(a) presents the distribution of equivalent strain in the pure Al sample after a single ECAP pass. As can be seen, the difference in the shape of specimen at the head and tail also shows that the deformation is inhomogeneous along the longitudinal direction. In order to quantify the degree of strain inhomogeneity, the coefficient of variance of the equivalent strains, *CV*, introduced by Patil et al. is used [16]. The coefficient of variance of the equivalent strains is defined as

$$CV = \frac{\mathrm{Stdev}\,\varepsilon}{\varepsilon_{\mathrm{ave}}} \ , \tag{2.4}$$

where $\mathrm{Stdev}\,\varepsilon$ is the standard deviation of equivalent strain and $\varepsilon_{\mathrm{ave}}$ is the average of the equivalent strains along a chosen section of the specimen.

2.3 Results and Discussion

2.3.1 Influence of the Position of Ti in Matrix on Strain Inhomogenity along Ti

In order to determine the best position for embedding Ti in the host material, three different positions were considered. As the initial structure, two types of specimen shown in Fig. 2.3 are considered in this simulation. Figures 2.4(c) and (b) show the deformed geometry and the distribution of the equivalent strain in specimen H1 with Ti embedded in the middle after a single ECAP pass, respectively. As can be observed, the deformation and the strain distribution are inhomogeneous in both the longitudinal direction and transverse direction. Moreover, it is seen from Fig. 2.4(c) that the amount of shear strain in Ti is less than that in the host matrix.

Figure 2.6 shows strain distributions along the neutral axis of the specimen for sample H1 and FGM2. Figures 2.6(a), (b), and (c) are results obtained for specimens in which Ti is embedded at the front end, in the middle, and at the rear end of the specimen, respectively. For comparison, the strain distributions in specimen without Ti are also shown in those figures. In the case of the specimen without Ti, strain distribution along the neutral axis is relatively homogeneous. On the other hand, equivalent strains in samples H1 and FGM2 drastically dropped in the part with Ti, and the strain distribution in another region is similar to that of Al without Ti. Comparing the strain distributions in Ti between H1 and FGM2, it is found that Ti embedded in the middle has the most homogeneous strain distribution and the highest equivalent strain. Therefore, it can be concluded that the middle part in the host material of an ECAPed specimen is the appropriate position to induce SPD in a difficult-to-work material.

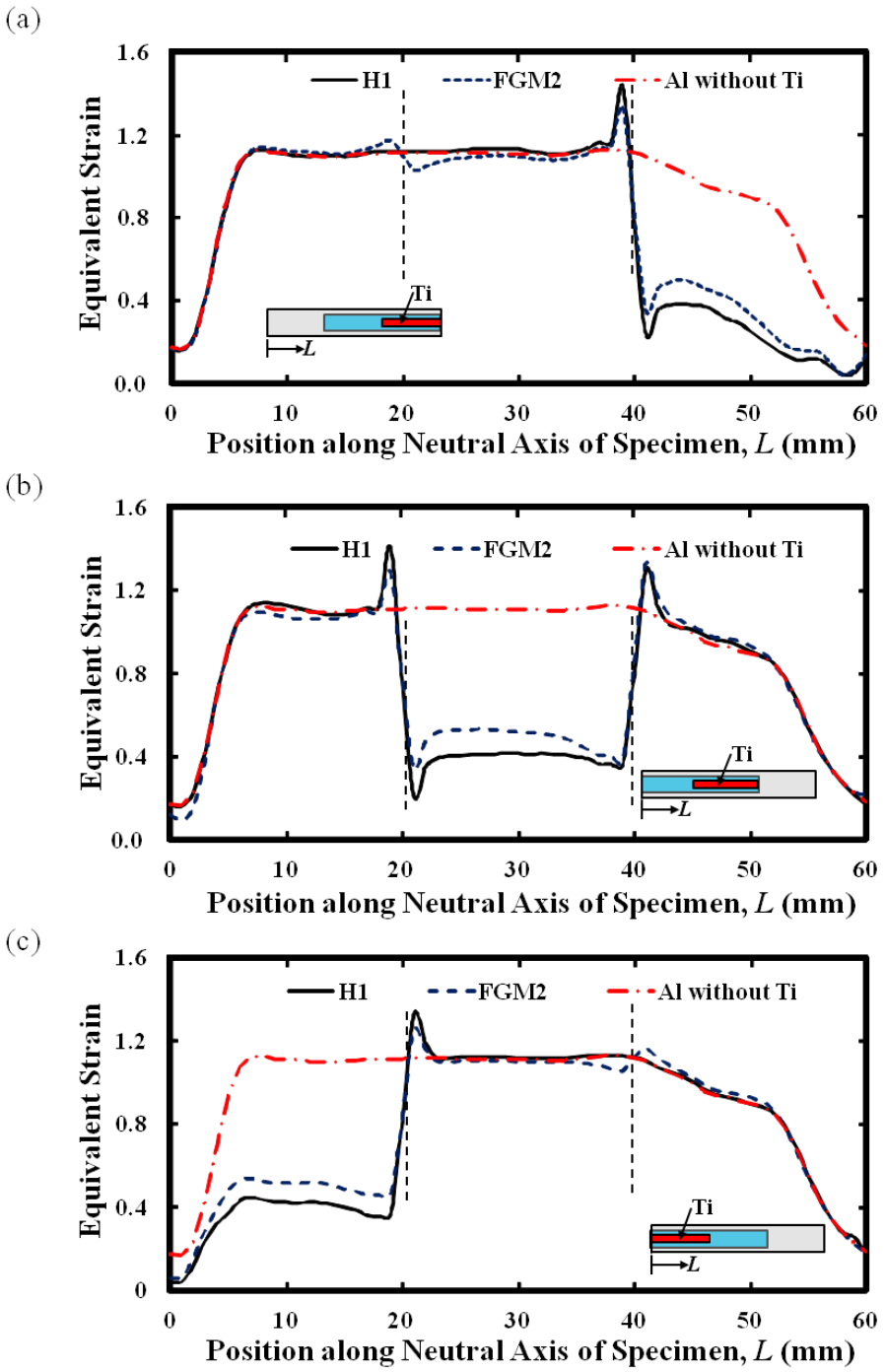

Fig. 2.6 Variation of equivalent strain along neutral axis of specimen with Ti in different positions: (a) at the front end, (b) in the middle, and (c) at the rear end. The schematic illustrations in graphs show the position of Ti. The dash lines indicate the interface between alloys.

2.3.2 Influence of the Host Material on Strain Inhomogeneity along Ti

To investigate the effect of the properties of the host material, FEM analysis was carried out using a different host material, as shown in Table 2.1. Figure 2.7 presents variation of equivalent strain inside Ti as a function of the normalized distance along Ti shown in Fig. 2.3. Figures 2.7(a) and (b) are ECAPed specimens with host materials of the homogeneous matrix (H1, H2 and H3) and composite matrix (FGM1, FGM2, and FGM3), respectively. Comparing the strain distributions along Ti embedded into homogeneous and FGM host materials, the strain distribution along Ti in FGM host materials is more homogeneous than that in the specimen with homogeneous materials. Also, the equivalent strain along Ti in the specimen with FGM host materials is relatively higher than that in the specimen with homogeneous materials. From these results, it is found that FGM is better than a homogeneous material as the host material in ECAP.

Moreover, it is found that the strain distributions of Ti in H3 and FGM3 show almost no difference and only show a small difference from that of Ti in FGM2. For these three specimens, Ti is embedded in the same inner layer material (Al-10%Ti) and is distinguished by the outer layer material. The outer layer materials of H3, FGM3, and FGM2 are Al-10%Ti, Al-5%Ti, and Al, respectively. Because FGM3 has almost similar strengths of the outer and inner layer materials, the strain distribution of Ti in FGM3 becomes similar to that in H3. On the other hand, a significant difference in the strength between the outer and inner layer materials of FGM2 gives a different strain distribution of Ti. These results show the significance of the gradient in strength of the host material.

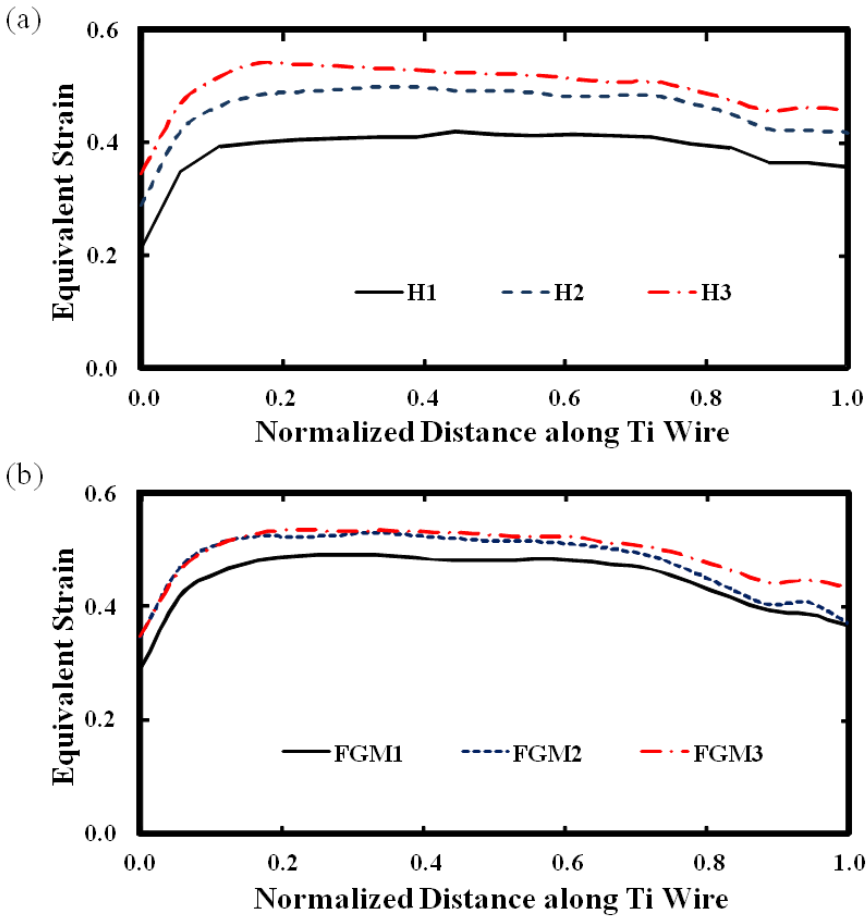

Fig. 2.7 Variation of equivalent strain along Ti: (a) embedded into homogeneous matrix and (b) embedded into composite matrix.

2.3.3 Effect of Die Geometry

The amount of strain in the specimen deformed by ECAP strongly depends on the shape of the die channel. In order to study this effect, an angle $\phi = 90°$ and different outer fillet radii R were considered. Also, the strain distributions of Ti in the specimen prepared using an ECAP die with an outer fillet radius R = 5.15 mm with $\phi = 90°$, $\phi = 105°$, and $\phi = 120°$ were studied.

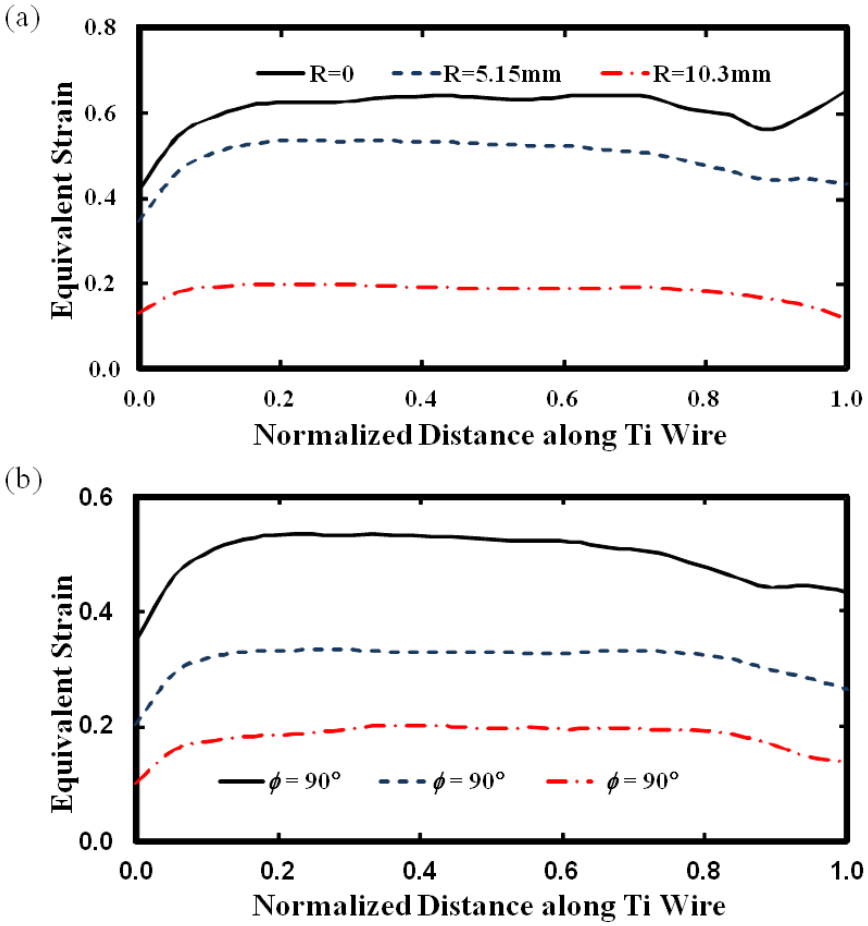

Fig. 2.8 Variation of equivalent strain along Ti embedded into FGM3: (a) with different outer fillet radii, R and (b) with different die angles, ϕ.

Figures 2.8(a) and (b) show the variation of equivalent strain along Ti with different die outer filler radii, R, and die angle, ϕ, respectively. When the angle of the die channel is fixed, the strain induced in Ti is increased by reducing R. On the other hand, a die with ϕ increment reduces the strain induced in Ti. From these results, it is found that the strain of Ti is controlled by die geometry.

Average equivalent strain, ε_{ave}, and coefficients of variance of the equivalent strains, *CV*, along Ti were calculated for each specimen. For comparison, only Ti embedded into

H2 and FGM3 at different die outer fillet radii, R, and die angles are shown in Table 2.2. The strain inhomogeneity decreases as the die outer fillet radii or die angle decreases.

Table 2.2 Average equivalent strain ε_{ave} and coefficient of variance of the equivalent strain *CV* (Eq. (2.4)) along Ti embedded into H2 and FGM3.

ϕ (°)	R (mm)	H2		FGM3	
		ε_{ave}	*CV*	ε_{ave}	*CV*
90	0	0.564	0.108	0.605	0.089
90	5.15	0.459	0.110	0.493	0.102
90	10.3	0.164	0.145	0.178	0.133
105	5.15	0.281	0.109	0.313	0.107
120	5.15	0.156	0.158	0.179	0.148

2. 4 Conclusions

FEM analysis is successfully carried out in order to investigate the deformation of a difficult-to-work material during the single ECAP pass at ambient temperature. It is possible to induce SPD into the difficult-to-work material at ambient temperature using the proposed technique. The selection of the host material is very important. In the case of SPD of Ti, an Al-based alloy or Al-based FGM should be selected as the host material. Apart from that, the position for embedding the difficult-to-work material and the die geometry are important factors for its SPD. For SPD of Ti using ECAP, it is suggested that Ti is embedded in the middle of the Al-based FGM host material and that an ECAP die with an outer fillet radius R = 5.15 mm and $\phi = 90°$ is used.

References

1) V. M. Segal, V. I. Reznikov, A. E. Drobyshevski, and V. I. Kopylov: Russ. Metall. **1** (1981) 99.
2) R. B. Figueiredo, P. R. Cetlin, and T.G. Langdon: Acta Mater. **55** (2007) 4769.
3) S. L. Semiatin, V. M. Segal, R. E. Goforth, N. D. Frey, and D. P. DeLo: Metall.Mater. Trans. A **30** (1999) 1425.
4) I. Kim, W. S. Jeong, J. Kim, K. T. Park, and D. H. Shin: Scr. Mater. **45** (2001) 575.
5) D. H. Shin, I. Kim, J. Kim, Y. S. Kim, and S. L. Semiatin: Acta Mater. **51** (2003) 983.
6) A. Balakrishnan, B. C. Lee, T. N. Kim, and B. B. Panigrahi: Trends Biomater. Artif. Organs **22** (2008) 54.
7) A. Balyanov, J. Kutnyakova, N. A. Amirkhanova, V. V. Stolyarov, R. Z. Valiev, X. Z. Liao, Y. H. Zhao, Y. B. Jiang, H. F. Xu, T. C. Lowe, and Y. T. Zhu: Scr. Mater. **51** (2004) 225.
8) G. I. Raab, E. P. Soshnikova, and R. Z. Valiev: Mater. Sci. Eng. A **387-389** (2004) 674.
9) S. Jamian, Y. Watanabe, H. Sato, and E. Miura-Fujiwara: presented at 20th Functional Graded Material Symp. (FGM2009), 2009.
10) Y. L. Yang and S. Lee: J. Mater. Process. Technol. **140** (2003) 583.
11) Y. Iwahashi, J. Wang, Z. Horita, M. Nemoto, and T. G. Langdon: Scr. Mater. **35** (1996) 143.
12) S. Li, M. A. M. Bourke, I. J. Beyerlein, D. J. Alexander, and B. Clausen: Mater. Sci. Eng. A **382** (2004) 217.
13) C. J. Luis, P. Gonzalez, and Y. Garces: J. Mater. Process. Technol. **143-144** (2003) 506.
14) H. S. Kim, M. H. Seo, and S. I. Hong: J. Mater. Process. Technol. **113** (2001) 622.
15) H. S. Kim, S. I. Hong, and M. H. Seo: J. Mater. Res. **16** (2001) 856.
16) V. Patil Basavaraj, U. Chakkingal, and T. S. Prasanna Kumar: J. Mater. Process. Technol. **209** (2009) 89.

Chapter 3

Experimental Study on Severe Plastic Deformation of Ti by Novel Equal-Channel Angular Pressing

3.1 Introduction

Equal-channel angular pressing (ECAP) process is preferred because a large plastic strain can be induced without any change in cross-sectional shape of the billet. Because of this, the deformation for the specimen can be repeated for huge strains. The multiple passes make it possible to induce different strains depending on the processing route [1–3]. The processing routes involved are, route A (no rotation), route B_A (90° back and forth rotation between passes), route B_C (90° in the same direction between passes), and route C (180° in the same direction between passes). Therefore, ECAP can induce huge strain by controlling the processing route.

However, severe plastic deformation (SPD) of Ti and Ti alloys at ambient temperature by ECAP is very difficult due to their ductility [1]. When Ti and Ti alloys are deformed by ECAP, the ECAP processing is carried out under high temperatures [1, 3–10]. This is because Ti and Ti alloys are difficult to deform due to hexagonal close packed (hcp) structure [1, 5]. In previous studies, the ECAP process for Ti has been performed under elevated temperatures up to 450 °C and it has been suggested that the lowest temperature for the successful deforming of Ti is 200 °C [7]. These studies show that it is very difficult to deform Ti by ECAP at ambient temperature.

Several recent reports have demonstrated that it is possible to deform Ti through multiple passes of ECAP at ambient temperature by increasing the channel angle up to 120°, under the processing speed of 2 mm/s [11–13]. For ECAP carried out in these studies, a special graphite lubricant containing ~15% MoS_2 powder was used. Based on these studies, it was reported that Ti was successfully processed through up to eight passes with route B_C. On the other hand, the authors have proposed an alternative

technique in processing Ti by ECAP at ambient temperature [14]. The proposed technique is the deformation of Ti by embedding a Ti wire into an easy-to-work material. In previous investigations, the deformation of Ti embedded in two different kinds of host material, namely homogeneous Al alloy and Al-based functionally graded material (FGM) with single-pass ECAP was carried out by the finite element method (FEM). Moreover, different positions of Ti embedded in the host material and different die geometry were considered. Based on the FEM results, an Al-based FGM matrix with the higher-strength alloy on the inner side was found to be a good host material. To reduce strain inhomogeneity along Ti, it has been suggested that Ti is embedded in the middle part in the host material and that an ECAP die with an outer fillet radius R = 5.15 mm and the two intersecting channels meeting at an angle 90° is used [14]. However, the workability of this technique is still questionable as no experimental work has been carried out so far. Moreover, the FEM was carried out only for a single ECAP pass and no data are available for multiple passes.

In this study, an experimental work using novel technique is carried out. Ti wire is tightly encapsulated in a hollow of host material made of Al-based FGM. ECAP is performed under route A for up to eight passes. Effects of the ECAP process and the host material on the microstructure and the hardness of Ti are discussed.

3.2 Experimental Procedure

3.2.1 Preparation of FGM billet

Figure 3.1 shows a schematic illustration of the FGM billet used in this work. The annealed Ti is embedded in the middle of the host material. Pure Ti (99.5%) with a diameter of 1.5 mm and a length of 20 mm is annealed at 800 °C for 5 min using a vacuum furnace. Pure Al (99.99%) and Al-Al_3Ti alloys are chosen as an outer layer and inner layer of the host materials, respectively.

4.5 Conclusions

A new design of crash box with stepwise strength gradient in longitudinal directions has been successfully proposed. The crash behavior of FGM crash boxes with different stepwise strength gradients were investigated using FEM. The results of numerical simulations showed that the crash or folding patterns can be pre-determined by using FGMs. High crash energy absorption can be achieved by the proposed FGM crash box. Moreover, it is shown that the energy absorption characteristics of crash box are changed with different stepwise strength gradient in FGMs and the cross-sectional shape of the crash box. In designing an FGM crash box for certain purpose, the stepwise strength gradient in FGMs and/or the cross-sectional shape of the crash box can be changed depends on the type of loading. For an example, the stepwise strength gradient FGM2, which gives high crash force efficiency and low load fluctuation, is recommended for the crash box under the quasi-static load. In contrast, for the cross-sectional shape of the crash box under the same loading condition, hexagonal is recommended.

References

1) K.S. Bae: Front structure for car body. United States Patent (2009) US007533913 **B2**.
2) H. R. Zarei, M. Kroger, and H. Albertsen: Compos. Struct. **85** (2008) 245.
3) J. S. Kim, H.J. Yoon, and K.B. Shin: Adv. Compos. Mater. **20** (2011) 385.
4) H. S. Kim: Thin-Walled Struct. **40** (2002) 311.
5) J.S. Qiao, J.H. Chen, and H.Y. Che: Thin-Walled Struct. **44** (2006) 692.
6) A. Rusinek,R. Zaera, P. Forquin, and J.R. Klepaczko: Thin-Walled Struct. **46** (2008) 1143.
7) M. Langseth,O.S. Hopperstad, and T. Berstad: Int. J. Impact Eng. **22** (1999) 829.
8) Y. Nakazawa, K. Tamura, M. Yoshida, K. Takagi, and M. Kano: in Onate, E.,Owen and D.R.J. (Eds.): Proceedings of the VIII International Conference on Computational Plasticity (COMPLAS VIII), Barcelona (2005) p. 167.

9) K. Tamura, Y. Nakazawa, M. Yoshida, K. Takagi, and M. Kano: Bull. Iron Steel Inst. Japan **16** (2011) 369. (*in Japanese*).
10) A.G. Mamalis, D.E. Manolakos, M.B. Ioannidis, D.G. Chronopoulos, and P.K. Kostazos: Comp. Struct. **89** (2009) 416.
11) J. Bi, H. Fang,Q. Wang, and X. Ren: Finite Elements in Analysis and Design **46** (2010) 698.
12) S. Santosa and T. Wierzbicki: Comput. Struct. **68** (1998) 343.
13) H.W. Song, Z.J. Fan, G. Yu, Q.C. Wang, and A. Tobota: Int. J. Solid Struct. **42** (2005) 2575.
14) G. Sun, G. Li, S. Hou, S. Zhou, W. Li, and Q. Li: Mater. Sci. Eng. A **527** (2010) 1911.
15) L. Peroni, M. Avalle, and G. Belingardi: Int. J. Impact Eng. **36** (2009) 498.
16) N. Gupta and W. Ricci: Mater. Sci. Eng. A **427** (2006) 331.
17) S. Kiernan, L. Cui, and M.D. Gilchrist: Int. J. Non-Linears Mech. **44** (2009) 456.
18) A.H. Brothers and D.C. Dunand: Mater. Sci. Eng. A **489** (2008) 439.
19) M. Fujda, R. Mišičko, L. Rusňáková, and M. Sojko: J. Metal. Mater. Miner. **17** (2007) 35.
20) H. Hooputra, H. Gese, H. Dell, and H. Werner: Int. J. Crash **9** (2004) 449.
21) ABAQUS analysis user manual. Version 6.8. Dassault Systemes 2008.